Analysis of fully developed mixed convection in open-ended annuli with viscous dissipation

N. Girish[1] · M. Sankar[2] · Keerthi Reddy[2]

Abstract

The vertical, open-ended double-passage annular space between three vertical concentric co-axial cylinders is an important geometry representing significant number of industrial applications. For a design engineer, the knowledge of fully developed mixed convection in this geometry is very essential. Hence, in this paper, it is proposed to numerically as well as analytically investigate the fully developed mixed convective flow in the vertical annuli having two annular passages with open upper and lower boundaries by taking viscous dissipation into consideration. The prime objective of the analysis is to bring out the influences of the location of middle cylinder, known as baffle, and viscous dissipation on the fluid flow and temperature profiles as well as the associated thermal transport rates. By neglecting the viscous dissipation influences, exact solutions are determined, while the finite difference-based numerical solutions are achieved in the presence of viscous dissipation. Further, excellent agreement is obtained between the analytical and numerical solutions under limiting conditions. The roles of viscous dissipation and baffle location are meticulously brought out through the flow pattern, temperature profiles and heat transport rates.

List of symbols

Br	Brinkman number
C_f	Skin friction coefficient
D	Diameter of annulus
g	Acceleration due to gravity
Gr	Grashof number
GR	Modified Grashof number
h	Heat transfer coefficient
k	Thermal conductivity
N	Baffle position
Nu	Nusselt number
p	Pressure
q	Mass flow rate
Re	Reynolds number
r_i	Radius of inner cylinder
r_m	Radius of middle cylinder
r_o	Radius of outer cylinder
T	Dimensional temperature
r, z	Dimensional radial and axial coordinates
R, Z	Dimensionless radial and axial coordinates
u, v	Velocity components in radial and axial directions
V	Dimensionless axial velocity
v_r	Reference velocity

Greek symbols

β	Volumetric coefficient of thermal expansion
γ	Pressure gradient
μ	Viscosity
λ	Radius ratio
ν	Kinematic viscosity
θ	Dimensionless temperature
ρ	Density

Subscripts

1	Inner passage
2	Outer passage
b	Bulk temperature
c	Cold wall
h	Hot wall

✉ M. Sankar
  manisankariyer@gmail.com

1 Department of Mathematics, JSS Academy of Technical Education, Bengaluru, India

2 Department of Mathematics, School of Engineering, Presidency University, Bengaluru, India

Introduction

Buoyancy-driven convection in open-ended, double-passage geometries have been the topic of many investigations until recently, since the outcomes could serve as an important supplementary data for the design of passive solar heating, electronic components cooling and many more applications. Among these geometries, a vertical annular space open at both ends portrays a basic configuration for the above applications. Further, the convective flows and heat transport processes in the annular space intensely depend on the location of middle cylinder and curvature ratio.

Fully developed mixed convective flow and the associated heat transport properties have been investigated both analytically and numerically by many researchers with or without viscous dissipation. The analysis is carried out in various geometrical spaces, such as parallel plates, upright tubes, annular space designed by co-axial tubes and double-passage conduits under diverse thermal boundary conditions. For fully developed situations, McBain [1] found exact solutions for buoyant convection in tall cavities of rectangular and elliptic cross section using parallel flow assumptions. Analytical solutions are obtained by El-Din [2] for fully developed laminar forced convection to study the influence of thermal and mass buoyancy forces in vertical channel and criteria for flow reversal is also derived. Guo et al. [3] suggested various ways to enhance the heat transfer namely, changing the thermal boundary condition and using special inserts. The significance of Brinkman number on heat transfer in micro-channels was explored by Tso and Mahulikar [4] for single phase forced convection, who found that Nusselt number may correlate with Brinkman number for rectangular micro-channels. Barletta [5] analyzed fully developed mixed convection for both symmetric and asymmetric thermal conditions in a vertical channel using perturbation series method and predicted that the flow reversal is enhanced with viscous dissipation in descending flow whereas it reduces the upward flow for asymmetric thermal case. In a vertical passage, the influence of reference temperature on fully developed buoyant flow is studied by Barletta and Zanchini [6] for various temperature conditions. The reference temperature influences velocity profile and the pressure gradient significantly. Barletta and Zanchini [7] obtained analytical solution for fully developed laminar mixed convection using perturbation method in a vertical inclined channel by considering effect of viscous dissipation; results reveal that viscous dissipation improves the effect of buoyancy and vice versa.

Fully developed mixed convective flow through a microchannel is studied by Avci and Aydin [8] by taking slip velocity and thermal jump into account and derived closed-form solutions and heat transport correlations. By considering three types of thermal conditions for a fully developed situation, Umavathi and Chamkha [9] analyzed the mixed convection in upright channel by taking heat source or heat sink into account. Analytical results are presented either neglecting viscous dissipation or buoyancy force; however, model equations are numerically solved when viscous dissipation is considered. Idowu et al. [10] investigated effects of buoyancy and viscous dissipation on laminar convection with transpiration using perturbation method with uniform and asymmetric wall temperatures in a vertical channel. Results reveal that buoyancy and viscous dissipation promotes flow in case of downward flow but lowers in case of upward flow. The combined influence of non-uniform thermal gradient and viscous dissipation on linear stability of buoyant flow in a horizontal infinite porous layer is performed by Roy and Murthy [11]. To augment or intensify the convective flows and associated thermal transport in a vertical plate channel, investigations are performed with different nanofluids and by considering the effects of magnetic field, porosity and viscous dissipation [12, 13]. Smith and Nochetto [14] presented numerical simulations using COMSOL for developing convective flows in rectangular and parallel plate channels and found good agreement with literature data on similar findings.

For laminar buoyant flow through an upright tube having constantly maintained hot or cold thermal cylindrical surfaces, Mortan [15] determined closed-form solution under the assumption of fully developed flow. Considering viscous dissipation into account, Barletta [16] studied laminar forced convection of power-law fluid in circular duct under fully developed assumption. Asymptotic behavior of temperature as well as asymptotic Nusselt number is presented for axial wall heat flux distribution, which is responsible for thermally developed region. Barletta [17] investigated mixed convective heat transfer using perturbation method in a vertical tube considering effect of viscous dissipation as well as buoyancy force, where tube is maintained with uniform temperature. Lee [18] obtained analytical solution for natural convective heat and mass transfer by considering flow to be fully developed in a partially heated vertical circular duct with uniform wall temperature and concentration, uniform heat and mass flux. Jha et al. [19] investigated fully developed unsteady buoyant convection of viscous reactive fluid in a straight cylinder. Applying perturbation technique, exact solutions are derived for steady-state flow, whereas using finite difference method numerical solutions are found for transient flow.

In an upright annular space, fully developed mixed convective flow is analyzed by Rokerya and Iqbal [20] for different thermal conditions. Exact expressions for velocity and temperature are derived for zero viscous dissipation case while the Runge–Kutta method of fourth order is preferred as dissipation effects are considered. Prakash and Renzoni [21] numerically investigated the influence of buoyancy and radial fins for fully developed convection in vertical

annulus. Fins are fixed on outer surface of inner wall of the annuli, and they predicted that both buoyancy and radial fins enhance thermal transport. To study the influences of temperature-dependent fluid properties, Herwig and Klemp [22] investigated fully developed laminar flow in concentric annulus by maintaining both walls of the annulus with constant heat fluxes. Considering four fundamental boundary conditions, El-Shaarawi and Al-Nimr [23] studied free convection in vertical concentric annuli under fully developed situation. Analytical expression for velocity, thermal fields are obtained for all four fundamental boundary conditions and also show that solutions are limiting case for developing flow. Transient fully developed free convection is analytically studied by Al-Nimr [24] in an open-ended vertical concentric annulus and derived the expressions for velocity, temperature and Nusselt number. Fully developed heat transfer of Newtonian fluids of very high viscosity is examined by Coelho and Pinho [25] in concentric annuli by imposing asymmetric constant wall temperatures and constant heat fluxes.

Jha et al. [26] made both analytical and numerical investigations of fully developed unsteady and steady free convective flow in a vertical annulus for reactive viscous fluid. Analytical expressions are derived for velocity, temperature, skin friction as well as heat transfer rate. Fully developed free convection has been examined by Jha et al. [27] in a vertical annular micro-channel and obtained an exact solution for temperature-dependent viscosity by considering not only velocity slip but also temperature jump at the surfaces of micro-channel. Results reveal that enhancement of fluid velocity, velocity slip, volume flow rate and skin friction can be attained by increasing the viscosity variation parameter. Recently, for fully developed flow conditions, Sankar et al. [28] presented a detailed analysis of mixed convective thermal transport in double-passage annular spaces by considering viscous dissipation, porosity and magnetic field. It was shown that the baffle location and viscous dissipation act as vital parameters to control the convective flow and thermal transport processes in both passages. Later, Girish et al. [29, 30] performed numerical simulations for developing convective flow and thermal transport in vertical double-passage annuli. Theoretical and experimental investigations of fluid flow and thermal transport phenomena occur in double-pipe heat exchangers that have also been paid attention in the literature [31–33].

Mixed convective flow under fully developed condition is analytically examined by El-Din [34] in vertical channel, designed from three parallel plates with middle plate assumed as perfectly conductive thin baffle/fin while other two walls are maintained with different temperatures. Expression for velocity in both the streams and temperature is derived, and also Nusselt number on outer walls has been evaluated. Later, in similar double-passage, El-Din [35] obtained analytical as well as numerical solutions of combined free-forced convective flow by assuming the flow to be fully developed. By taking viscous dissipation into consideration, El-Din [36] numerically investigated mixed convective flow in a uniformly heated vertical double-passage channel for fully developed case. The effects of baffle position, Brinkman number and mixed convection parameter on velocity and thermal fields are examined. Mixed convective flow of micropolar fluid has been investigated by Umavathi [37] to explore the effect of thin and perfectly conductive baffle in vertical channel under fully developed assumption. Author obtained analytical expression for velocity, microrotation velocity and temperature fields in both streams of the channel as well as criteria for occurrence of flow reversal. Recently, Ahmed et al. [38] analyzed the forced buoyant flow of power-law nanofluids in an annular section by considering two types of nanoparticle and found that Cu nanoparticle promotes thermal transport. Malvandi et al. [39] analyzed the impact of radial magnetic force on alumina-based nanofluid inside a horizontal annular geometry by including Navier's slip criterion for two different thermal conditions.

The influence of heat source lengths on buoyant convection in a vertical annulus has been analyzed by Mebarek-Oudina [40] for wide range of physical and geometrical parameters. Recently, Gourari et al. [41] made an attempt to investigate the effects of inclination angle of vertical annular enclosure on convective flow and thermal transport processes. In a vertical annulus, simulations for mixed convection nanofluid flow are attempted to explore the effects of an applied magnetic force by Shakiba and Rahimi [42] and Hekmat et al. [43]. Analytical solutions are found for constantly moving inner and outer cylinders in [42] while numerical results for 3D magnetic nanofluids are presented in [43]. Through extensive numerical simulations, Mebarek-Oudina and co-workers [44, 45] found that the discrete heating of annular enclosure wall enhances the heat transfer compared to complete heating of the enclosure wall. Singh and Makinde [46] performed numerical study of uniform slip flow along a stationary vertical cylinder and found that the shear stress and heat transfer rate are strongly influenced by slip parameter. Later, Makinde and co-workers [47, 48] analyzed thermal and entropy generation analysis of Couette flow in the annular space between two concentric pipes. Buoyant convection and the associated heat transport mechanism of nanofluid in a permeable cylinder filled with porous medium is studied by Khamis et al. [49] with Navier slip condition. Recently, Raza et al. [50] investigated the effect of magnetic field on convective flow of nanofluid by considering the different shape of nanoparticles.

The detailed survey on the available literature reveals no attempt is made on fully developed flow in an upright double-passage annular space structured through three co-axial
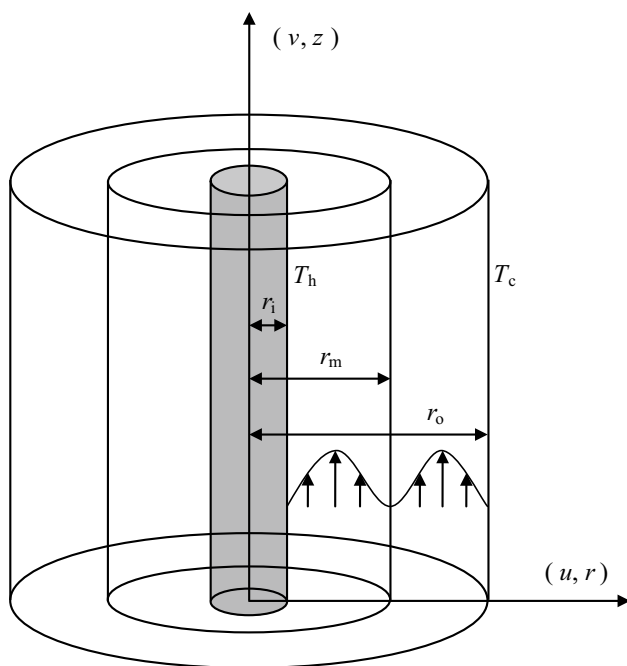
Fig. 1 Physical configuration and coordinate system

cylinders. However, the existing analyses on similar geometry are restricted to the vertical double-passage from parallel plates. Unfortunately, the simulations from parallel plate double-passage channel cannot be utilized for the applications involving double-passage annuli due to curvature effect. Hence, in this paper, fully developed mixed convective flow is numerically as well as analytically examined in the vertical double-passage annuli.

Problem statement and model equations

The geometrical structure and coordinate system used in this analysis, portrayed in Fig. 1, is the double annular passage designed through three vertical co-axial cylindrical pipes of which center thin cylinder is assumed to be perfectly conductive known as the baffle. In this double annular passage, r_i, r_m and r_o are, respectively, the radii of interior, center and exterior cylinders. The inner cylinder is maintained at hotter temperature compared to outer cylinder. It is also assumed that the center cylinder is thin and can be moved along radial direction. The flow is considered to be two-dimensional, laminar, incompressible and steady. All fluid properties, except density in body force term, are chosen as constant. In buoyancy term, the variation of density with respect to temperature is modeled through the Boussinesq approximation. Based on these hypotheses and by taking into account of viscous dissipation, the governing equations are [28, 30, 40]:

$$\frac{\partial u}{\partial r} + \frac{u}{r} + \frac{\partial v}{\partial z} = 0, \tag{1}$$

$$u\frac{\partial u}{\partial r} + v\frac{\partial u}{\partial z} = -\frac{1}{\rho_o}\frac{\partial p}{\partial r} + \nu\left[\frac{\partial^2 u}{\partial r^2} + \frac{1}{r}\frac{\partial u}{\partial r} + \frac{\partial^2 u}{\partial z^2} - \frac{u}{r^2}\right], \tag{2}$$

$$u\frac{\partial v}{\partial r} + v\frac{\partial v}{\partial z} = -\frac{1}{\rho_o}\frac{\partial p}{\partial z} + \nu\left[\frac{\partial^2 v}{\partial r^2} + \frac{1}{r}\frac{\partial v}{\partial r} + \frac{\partial^2 v}{\partial z^2}\right] + g\beta(T - T_r), \tag{3}$$

$$\rho Cp\left[u\frac{\partial T}{\partial r} + v\frac{\partial T}{\partial z}\right] = k\left[\frac{\partial^2 T}{\partial r^2} + \frac{1}{r}\frac{\partial T}{\partial r} + \frac{\partial^2 T}{\partial z^2}\right] + \mu\left(\frac{\partial v}{\partial r}\right)^2. \tag{4}$$

The mass conservation at a given cross section is represented by the following integral continuity equation [23]:

$$q = \pi\left(r_m^2 - r_i^2\right)v_r = \int_{r_i}^{r_m} 2\pi r v_1 \, dr$$

$$\text{and} \quad q = \pi\left(r_o^2 - r_m^2\right)v_r = \int_{r_m}^{r_o} 2\pi r v_2 dr. \tag{5}$$

The dimensional boundary conditions in both annular passages are [28, 34]:

$$\begin{aligned}
r = r_i, \quad & v_1 = 0, \quad T_1 = T_h \\
r = r_m, \quad & v_1 = 0 = v_2, \quad T_1 = T_2 \\
r = r_o, \quad & v_2 = 0, \quad T_2 = T_c.
\end{aligned} \tag{6}$$

To transform the governing equations and boundary conditions into dimensionless form, the following non-dimensional parameters are used.

$$\begin{aligned}
& R = \frac{r}{r_o}, \quad V = \frac{v}{v_r}, \quad Z = \frac{z}{r_o Re}, \\
& T_r = \frac{(T_c + T_h)}{2}, \quad \theta_j = \frac{T_j - T_r}{T_h - T_c}, \\
& P = \frac{p}{\rho_o v_r^2}, \quad Re = \frac{v_r r_o}{\nu}, \quad Gr = \frac{g\beta(T_h - T_c)r_o^3}{\nu^2}, \\
& Br = \frac{\mu v_r^2}{k(T_h - T_c)}, \quad N = \frac{r_m}{r_o}, \quad \lambda = \frac{r_i}{r_o}.
\end{aligned}$$

In the above equations, T_r represents reference temperature which is the average of inner and outer cylinder temperatures and v_r represents the reference velocity and is defined as $v_r = \frac{1}{r_o - r_i}\int_{r_i}^{r_o} v \, dr$.

Applying fully developed assumptions leads to vanishing transverse velocity and derivative of temperature in z direction. As such, we have $u = 0$, $\frac{\partial}{\partial z}() = 0$ and $\frac{\partial^2}{\partial z^2}() = 0$ and

using the non-dimensional variables given above, the model equations reduce to the following non-dimensional ordinary differential equations:

$$\frac{d^2 V_j}{dR^2} + \frac{1}{R}\frac{dV_j}{dR} = \frac{dP_j}{dZ} - GR\,\theta_j, \tag{7}$$

$$\frac{d^2\theta_j}{dR^2} + \frac{1}{R}\frac{d\theta_j}{dR} + Br\left(\frac{dV_j}{dR}\right)^2 = 0. \tag{8}$$

The dimensionless form of integral continuity equation in passages -1 and -2 are

$$\int_\lambda^N R V_1\,dR = \frac{1}{2}\left(N^2 - \lambda^2\right) \quad\text{and}\quad \int_N^1 R V_2\,dR = \frac{1}{2}\left(1 - N^2\right). \tag{9}$$

Here, $j = 1$ and 2 represents the first and second annular passages, respectively. Further, non-dimensional boundary conditions are:

$$\begin{aligned}
R &= \lambda, & V_1 &= 0, & \theta_1 &= 0.5 \\
R &= N, & V_1 &= 0 = V_2, & \theta_1 &= \theta_2 \\
R &= 1, & V_2 &= 0, & \theta_2 &= -0.5.
\end{aligned} \tag{10}$$

The present investigation has the following non-dimensional physical and geometrical parameters:

$GR = Gr/Re$ is the modified Grashof number,
$Br = \frac{\mu\, v_r^2}{k(T_h - T_c)}$ is the Brinkman number,
$N = \frac{r_m}{r_o}$ is the baffle position,
$\lambda = \frac{r_i}{r_o}$ is the radius ratio.

The quantitative measure in thermal transport analysis is the amount of heat transferred from thermally active walls and is measured by the dimensionless number known as Nusselt number. It is defined as

$$Nu = \frac{hD}{k}, \quad\text{where}\quad D = 2\left(r_o - r_i\right). \tag{11}$$

Also, the dimensionless form of local Nusselt number on the hot and cold walls is given as:

$$Nu_h = \frac{4(1-\lambda)}{\left(2\theta_{b1} - 1\right)\lambda \ln\lambda} \quad\text{and}\quad Nu_c = \frac{-4(1-\lambda)}{\left(1 + 2\theta_{b2}\right)\ln\lambda}. \tag{12}$$

In Eq. (12), θ_{b1} and θ_{b2} are, respectively, the non-dimensional bulk temperatures in the first and second annular passages and are given by

$$\theta_{b1} = \frac{\int_\lambda^N \theta_1 V_1 R\,dR}{\int_\lambda^N V_1 R\,dR} \quad\text{and}\quad \theta_{b2} = \frac{\int_N^1 \theta_2 V_2 R\,dR}{\int_N^1 V_2 R\,dR}, \tag{13}$$

where V_1, θ_1 and V_2, θ_2 are the velocity and temperature in the passages -1 and -2, respectively.

The skin friction coefficient C_f can be expressed as $C_f = \frac{\tau_{wall}}{\rho v_r^2/2}$. Using the non-dimensional variables, it takes the form $-\frac{C_f Re}{2} = \frac{dV}{dR}$. This quantity is calculated along the inner and outer cylinders for various parametric values.

Exact solutions

The model Eqs. (7) and (8) which describes the fully developed convective flow with viscous dissipation in the double annular passages are coupled and nonlinear in nature. These equations can be decoupled either by taking $Br = 0$ or $GR = 0$, that is, by neglecting the viscous dissipation or buoyancy force. First, the closed-form results are found by neglecting the viscous dissipation. Imposing the appropriate boundary conditions, Eqs. (7) and (8) are solved by taking $Br = 0$. The exact solutions for velocity and temperature for both annular passages are given below:

$$\theta = \frac{\ln R}{\ln\lambda} - 0.5, \tag{14}$$

$$\begin{aligned}
V_1 = \frac{GR}{8}&\left[\left(\frac{\ln(R/\lambda)}{\ln(N/\lambda)}\right)\left\{-\frac{2}{\ln\lambda}\begin{pmatrix}\lambda^2 - N^2\\ \lambda^2(\ln\lambda - 1)\\ -N^2(\ln N - 1)\end{pmatrix}\right\}\right.\\
&\left.-\frac{2R^2\ln R}{\ln\lambda} + R^2\left(1 + \frac{2}{\ln\lambda}\right) + \lambda^2\left(1 - \frac{2}{\ln\lambda}\right)\right]\\
&+\frac{\gamma_1}{4}\left[\left(\frac{\ln(R/\lambda)}{\ln(N/\lambda)}\right)\left(\lambda^2 - N^2\right)\\ +R^2 - \lambda^2\right],
\end{aligned} \tag{15}$$

$$\begin{aligned}
V_2 = \frac{GR}{8}&\left[\left(\frac{\ln R}{\ln N}\right)\left\{+\frac{2}{\ln\lambda}\left(1 + N^2(\ln N - 1)\right)\right\}\right.\\
&\left.-\frac{2R^2\ln R}{\ln\lambda} + \left(R^2 - 1\right)\left(1 + \frac{2}{\ln\lambda}\right)\right]\\
&+\frac{\gamma_2}{4}\left[\frac{\ln R}{\ln N}\left(1 - N^2\right) + \left(R^2 - 1\right)\right],
\end{aligned} \tag{16}$$

where N is baffle position and $\frac{dP_j}{dZ} = \gamma_j$. The values of γ_j in $j = 1$ and 2 are calculated using Eq. (9). The values of γ_1 and γ_2 are as follows:

$$\gamma_1 = \left[2(N^2 - \lambda^2) - \frac{GR A_1}{2} \right] \Big/ A_2 \quad \text{and}$$

$$\gamma_2 = \left[2(1 - N^2) - \frac{GR A_3}{2} \right] \Big/ A_4, \tag{17}$$

where

pressure. However, this situation can be resolved by utilizing the integral continuity equation given by (9). The second-order finite difference approximations are used to replace the derivatives into its equivalent finite difference approximations and the reduced difference equations are iteratively solved by successive point over relaxation (SPOR)

$$A_1 = \left[\begin{array}{l} \left\{ \frac{N^2}{2} \left(\ln(N/\lambda) - \frac{1}{2} \right) + \frac{\lambda^2}{4} \right\} \left(\frac{1}{\ln(N/\lambda)} \right) \left\{ \begin{array}{l} \lambda^2 - N^2 \\ -\frac{2}{\ln(\lambda)} \left(\lambda^2(\ln\lambda - 1) - N^2(\ln N - 1) \right) \end{array} \right\} \\ -\frac{1}{8\ln\lambda} \left\{ N^4(4\ln N - 1) - \lambda^4(4\ln\lambda - 1) \right\} \\ +\frac{1}{4} \left(1 + \frac{2}{\ln\lambda} \right) (N^4 - \lambda^4) + \frac{\lambda^2}{2} \left(1 - \frac{2}{\ln\lambda} \right) (N^2 - \lambda^2) \end{array} \right],$$

$$A_2 = \left[\left\{ \frac{N^2}{2} \left(\ln(N/\lambda) - \frac{1}{2} \right) + \frac{\lambda^2}{4} \right\} \left(\frac{\lambda^2 - N^2}{\ln(N/\lambda)} \right) + \frac{1}{4}(N^4 - \lambda^4) - \frac{\lambda^2}{2}(N^2 - \lambda^2) \right],$$

$$A_3 = \left[\begin{array}{l} \frac{1}{4\ln N} \left\{ 1 - N^2 + \frac{2}{\ln\lambda} \left(1 + N^2(\ln N - 1) \right) \right\} \left\{ N^2 - 1 - 2N^2\ln N \right\} \\ -\frac{1}{8\ln\lambda} \left\{ N^4 - 1 - 4N^4\ln N \right\} + \frac{1}{4} \left(1 + \frac{2}{\ln\lambda} \right) (2N^2 - 1 - N^4) \end{array} \right],$$

$$A_4 = \left[\left(\frac{1 - N^2}{4\ln N} \right) (N^2 - 1 - 2N^2\ln N) + \frac{1}{4}(2N^2 - 1 - N^4) \right].$$

Flow reversal can be observed near cold wall for sufficiently large value of $GR = Gr/Re$. The conditions for reversal flow in passages -1 and -2 are $\frac{dV_1}{dR}\big|_{R=N} < 0$ and $\frac{dV_2}{dR}\big|_{R=1} < 0$, respectively. Differentiating the velocity at walls, the criteria for flow reversal in both passages can be derived as $GR > \frac{2\gamma_1 A_5}{A_6}$ and $GR > \frac{2\gamma_2 A_7}{A_8}$ in passages -1 and -2, respectively, where

and Gauss elimination methods. The finite difference (FD) equations from the momentum equations are solved using Gauss elimination method, while the FD equations arising from energy equation is solved using SPOR iterative method. To choose an optimum relaxation parameter, several trail cases are performed and is obtained as 1.645 for faster convergence.

$$A_5 = \frac{(\lambda^2 - N^2)}{N\ln(N/\lambda)} + 2N,$$

$$A_6 = -\left[\begin{array}{l} \frac{\left((\lambda^2 - N^2) + (-2/\ln\lambda)\left(\lambda^2(\ln\lambda - 1) - N^2(\ln N - 1)\right) \right)}{N\ln(N/\lambda)} \\ +\left(\frac{-2}{\ln\lambda} \right)(N + 2N\ln N) + 2\left(1 + \frac{2}{\ln\lambda} \right)N \end{array} \right],$$

$$A_7 = \left(\frac{1 - N^2}{\ln N} \right) + 2,$$

$$A_8 = -\left[\frac{1}{\ln N} \left\{ 1 - N^2 + \frac{2}{\ln\lambda} \left(1 + N^2(\ln N - 1) \right) \right\} + \left(\frac{-2}{\ln\lambda} \right) + 2\left(1 + \frac{2}{\ln\lambda} \right) \right].$$

Numerical solution

Suppose the viscous dissipation is included in the analysis ($Br \neq 0$), the nonlinear and coupled model equations do not permit the analytical solution. Hence, in this case, the governing equations are solved using the finite difference technique. It is important to mention that the solution of momentum equation requires an additional equation due to the presence of unknown pressure. That is, we have one equation and two unknowns, namely the velocity and

The grid independency check is carried out with several tests to choose optimum grid sizes in the physical domain. For this, extreme velocity and Nusselt number are chosen as the sensitive quantities to examine the proper choice of grids. From a coarse grids of 61 to finer grids of 201 are used, and we have ensured to have equal number of grids in both annular passages. From the detailed examination, we found that a total of 201 grid points consisting of 101 grid points in both annular passages produces fairly accurate results and further increase in grids does not produce any

appreciable change in the sensitive variables. The bulk temperatures are numerically integrated using Simpson's rule.

Validation

The numerical results obtained from the present finite difference method are validated with present analytical solutions as well as with other standard benchmark results for similar analysis. The validation has been carried out in two stages. In first stage, the current numerical predictions are validated with the present analytical solutions by neglecting the effect of viscous dissipation ($Br = 0$) and portrayed in Fig. 2. The comparison of flow and thermal profiles between the analytical and numerical results exhibited in Fig. 2 portrays the good agreement among the two solutions. It can be observed that the velocity profile increases with GR. In both the passages, the temperature profiles remain invariant as energy equation is independent of GR. Next, in the absence of viscous dissipation, the Nusselt numbers at the hot and cold walls are calculated from both analytical expressions and numerical solutions and the comparison is shown in Table 1. The table reveals that the Nusselt numbers determined from numerical solutions are in excellent agreement with the analytical expressions at all values of the modified Grashof number.

Finally, the results for the vertical double-passage channel from three vertical parallel plates have also been simulated from this analysis and validated with the results of El-Din [35] in Fig. 3 with and without viscous dissipation. Here the baffle is kept at middle of the channel ($N = 0.5$). The Grashof number is fixed for $GR = 50$ and three different values of Brinkman number are considered, viz., $Br = 0$, 0.05 and 0.1. The results displayed in Fig. 3 show fairly good agreement among the present predictions and that of El-Din [35].

Results and discussion

This section primarily illustrate the effects of modified Grashof number, Brinkman number, baffle location and radius ratio on the fully developed convective flow and thermal transport rates in the two annular passages with and without viscous dissipation. We have covered vast range of physical and geometrical parametric values and their influences on flow and thermal profiles as well as thermal transport rate are analyzed in detail. For all simulations, the first annular passage varies from $R = \lambda$ to $R = 1$ and second annular passage is from $R = N$ to $R = 1$.

Effect of buoyancy force

The effects of buoyancy force on fluid flow, thermal field and heat transfer rate are discussed in this section. In this
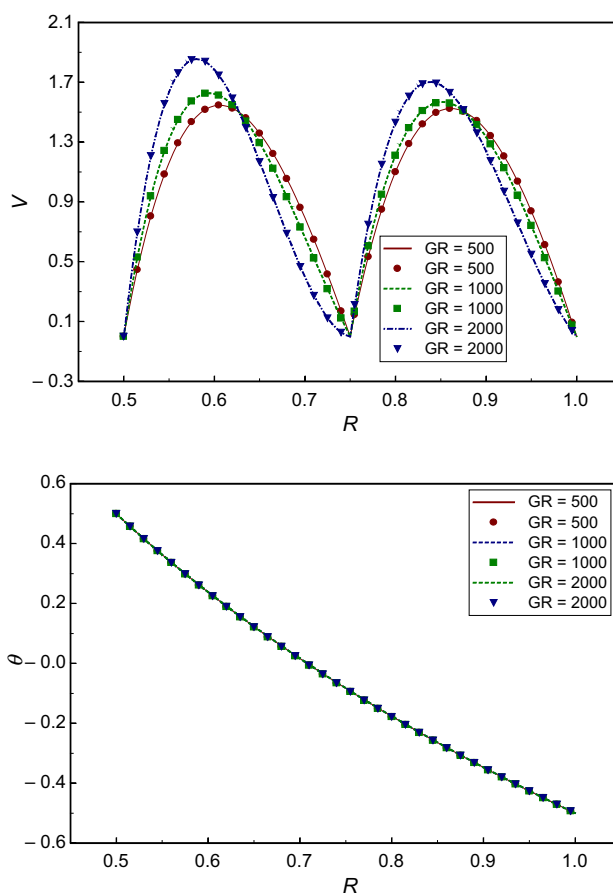

Fig. 2 Comparison of velocity (top) and temperature profiles (bottom) between the analytical and numerical results for $\lambda = 0.5$, $N = 0.75$, $Br = 0$ in the vertical double-passage annuli. Curves correspond to numerical results and symbols stands for analytical results

Table 1 Comparison of analytical and numerical values of Nusselt number on hot and cold walls for $Br = 0$, $\lambda = 0.5$ and $N = 0.75$ for different values of GR

GR	Nu_h		Nu_c	
	Analytical	Numerical	Analytical	Numerical
50	8.949912	8.937130	7.498241	7.503071
100	8.990172	8.977221	7.469628	7.474318
200	9.071790	9.058492	7.413052	7.417466
500	9.325784	9.311382	7.248353	7.251984
1000	9.782260	9.765781	6.989536	6.991999
1500	10.285724	10.266814	6.748565	6.750008
2000	10.843822	10.822047	6.523656	6.524206

analysis, the ratio between Grashof and Reynolds numbers is identified as the modified Grashof number and is denoted by GR. The collective effects of modified Grashof number, GR, and baffle position, N, on the flow and thermal profiles
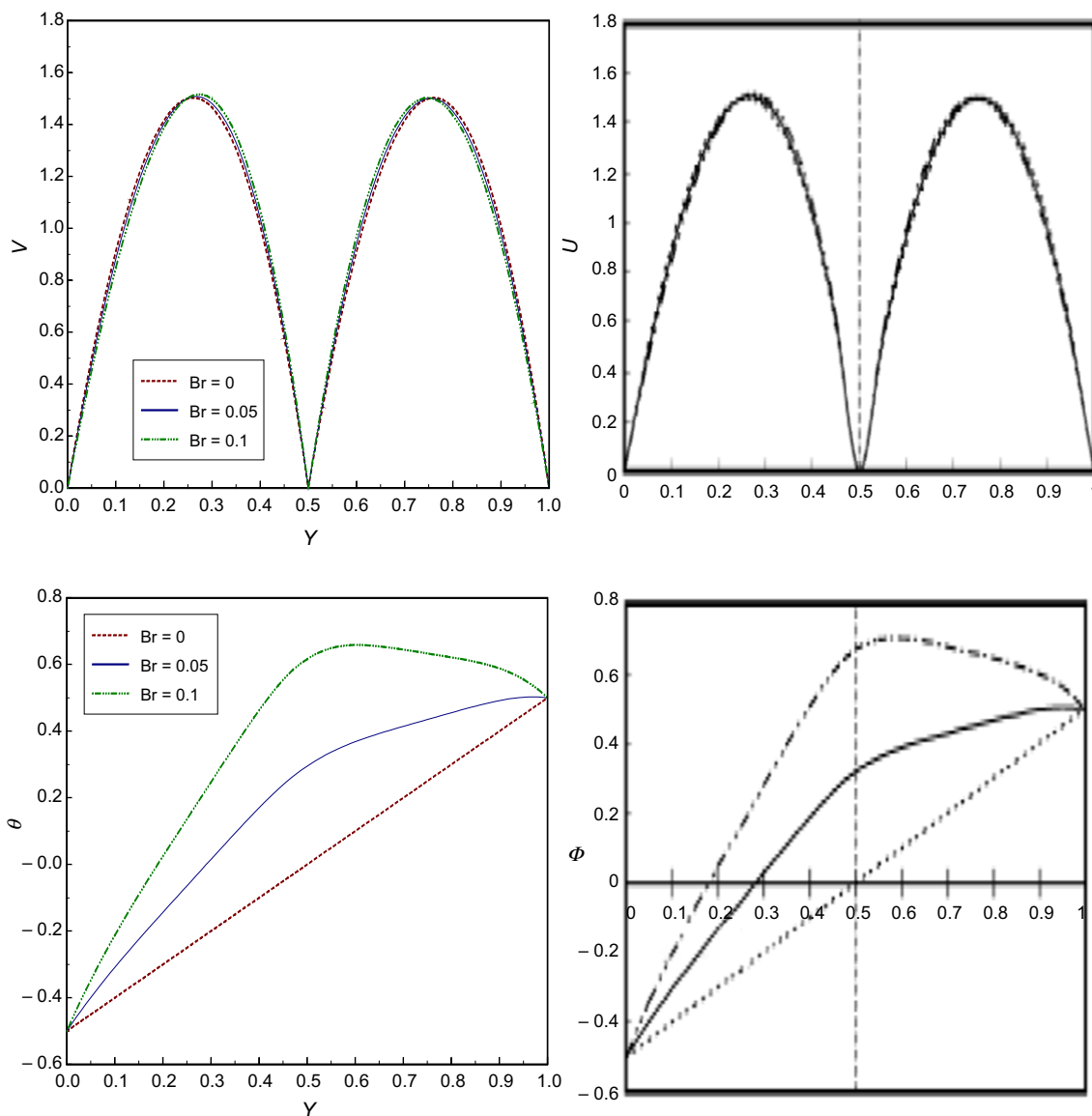
Fig. 3 Comparison of velocity (top) and temperature profiles (bottom) between present results (left) and the predictions of El-Din [35] (right) for a vertical double-passage parallel plate channel for $GR = 50$ and $N = 0.5$

is portrayed in Fig. 4 for fixed values of $\lambda = 0.5$, $Br = 0$. In particular, the velocity and temperature profiles are plotted for three baffle positions ($N = 0.6$, 0.75 and 0.9) and for each value of N, four different values of GR specifically 50, 500, 1000 and 2000 are varied. The observation of figure reveals that an increase in GR increases the magnitude of velocity, but the temperature profiles remains unchanged for all baffle locations and modified Grashof number, since the energy equation is independent of GR. As the modified Grashof number is increased, enhancement of mixed convective flow is clearly visible in both passages when baffle is positioned in center ($N = 0.75$). However, for the location of baffle either near hot wall ($N = 0.6$) or cold wall ($N = 0.9$), variation of velocity magnitude is significant only in wider passage

and velocity profiles in the narrow passage reveals meager variation. For $GR = 2 \times 10^3$, highest value of GR considered in this analysis, the maximum velocity is observed and the location of maximum velocity moves toward baffle for the baffle position $N = 0.6$, whereas it moves toward the hot wall for the case when baffle is located at 0.9. Another important observation from the results is the occurrence of flow reversal in the two annular passages. Interestingly, for sufficiently higher values of GR, the negative velocity or flow reversal is observed only when baffle is placed near the inner or outer wall. In particular, when baffle is placed near hot wall, flow reversal in passage -2 occurs near cold wall. However, for the placement of baffle near cold wall, the flow reversal in passage -1 occurs near the baffle.
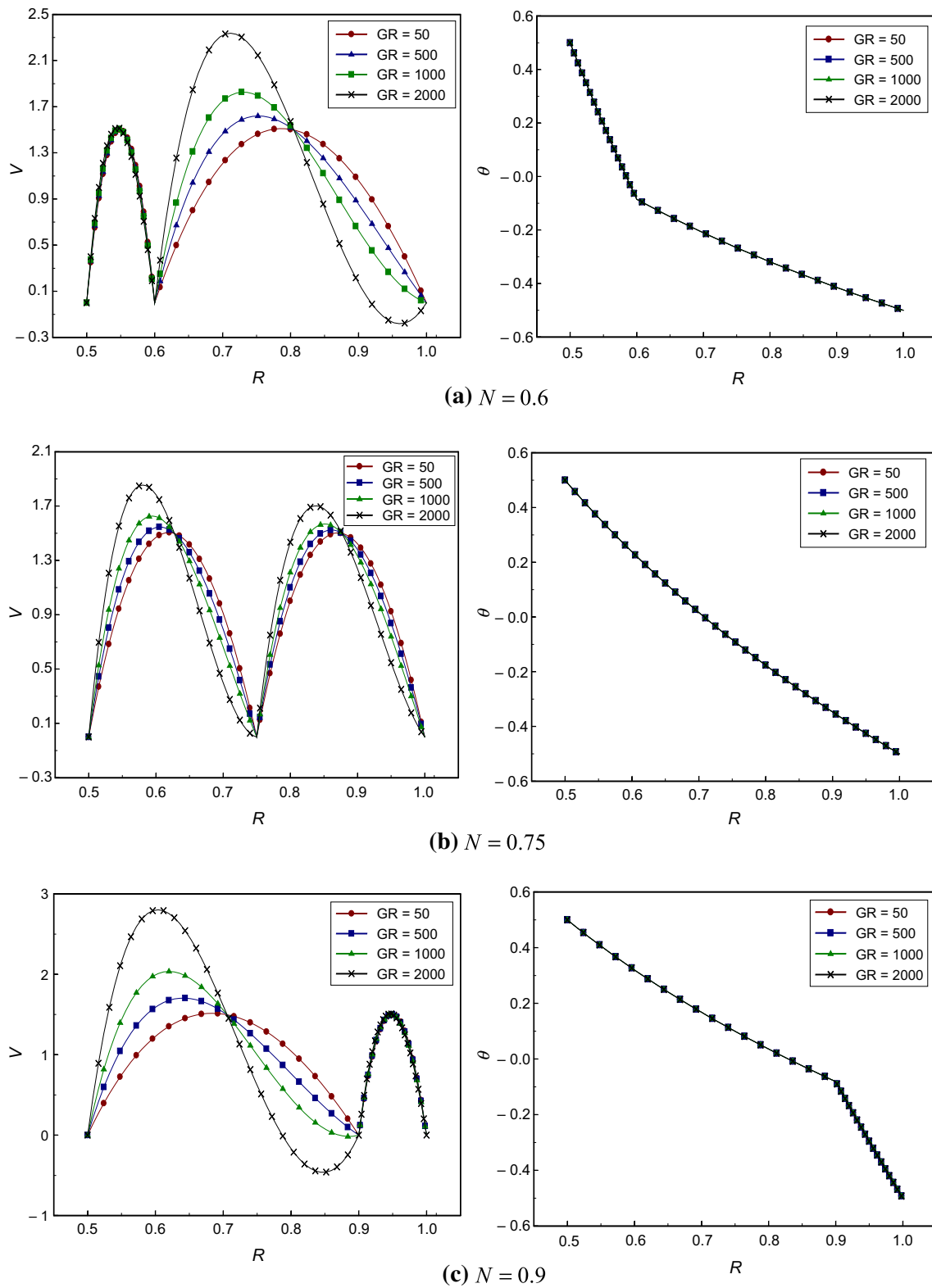
(a) $N = 0.6$

(b) $N = 0.75$

(c) $N = 0.9$

Fig. 4 Effect of GR and N on velocity and temperature profiles for $\lambda = 0.5$, $Br = 0$

(a) $\lambda = 0.1, N = 0.55$

(b) $\lambda = 0.3, N = 0.65$

(c) $\lambda = 0.5, N = 0.75$
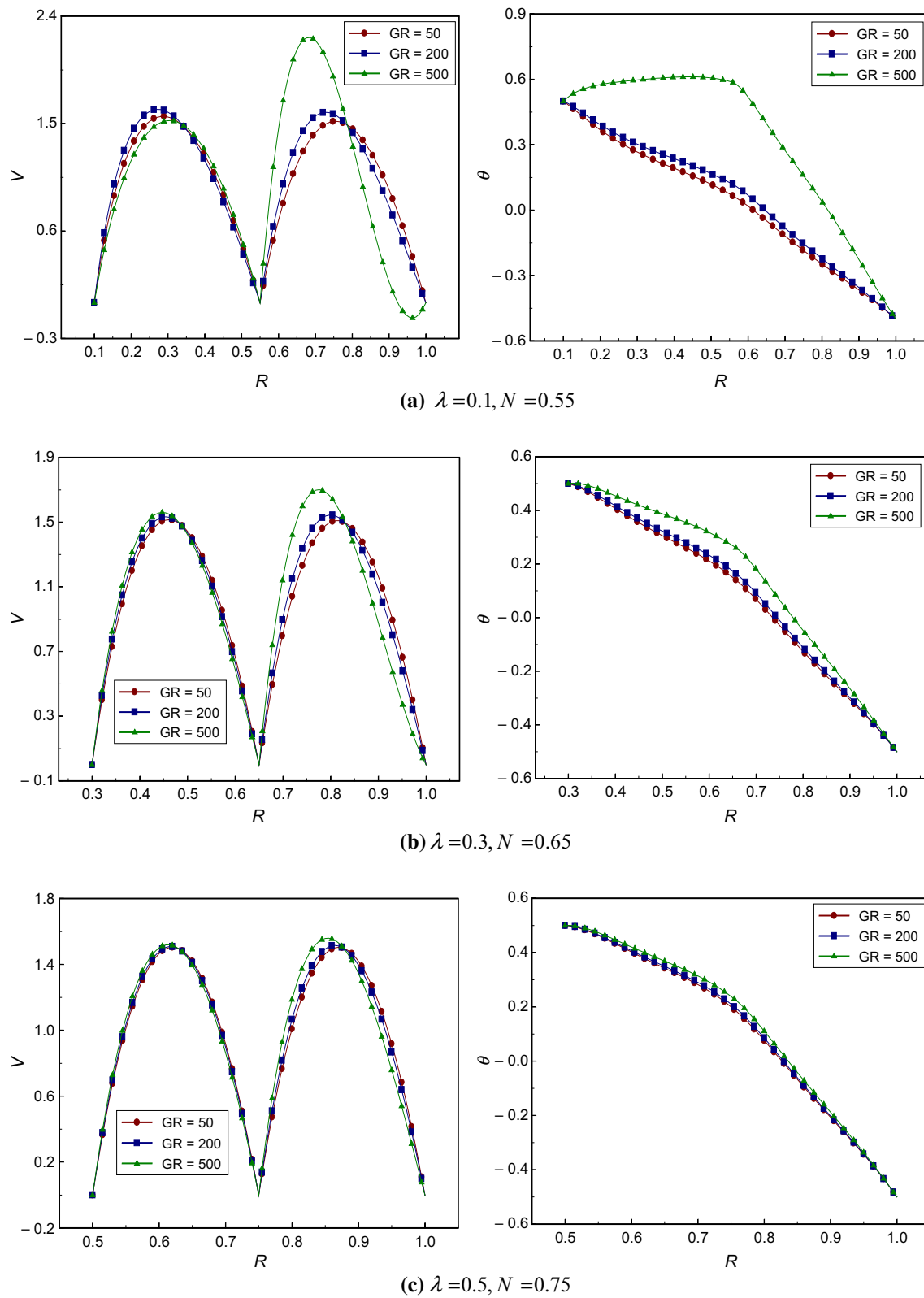
Fig. 5 Velocity and temperature profiles for $Br = 0.05$ and different values of λ, N and GR
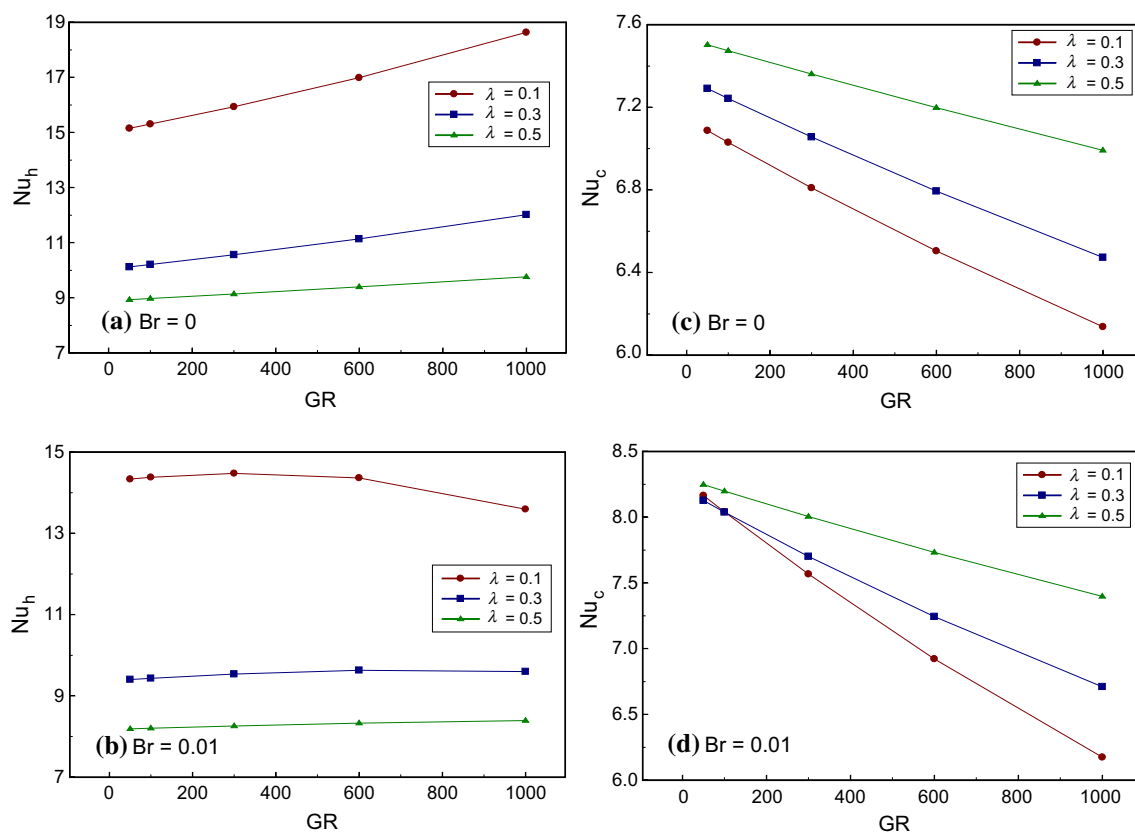
Fig. 6 Variation of hot wall $\left(Nu_h\right)$ and cold wall $\left(Nu_c\right)$ Nusselt numbers for different values of GR and λ at $Br = 0.0$ and $Br = 0.01$

The influence of modified Grashof number on velocity and thermal distributions for three values of radius ratio is presented in Fig. 5. To explore the impacts of radius ratio, three radius ratios are considered viz., $\lambda = 0.1$, 0.3 and 0.5. It is important to mention that an equal passage width is achieved, in all three radius ratios, by placing the baffle in middle of the annulus. As GR increases, velocity also increases in passage -2, but velocity variation in passage -1 is meager. For smaller radius ratio ($\lambda = 0.1$), maximum velocity and flow reversal is observed in passage -2. Also, due to the presence of viscous dissipation ($Br = 0.05$), temperature profiles reveal considerable variation. In particular, large variations are observed for smaller radius ratio and larger modified Grashof number.

Figure 6 portrays the collective effect of the physical and geometrical parameters, namely the modified Grashof number and radius ratio on heat transfer rate in the presence and absence of viscous dissipation. For this analysis, five representative values of GR and three representative values of radius ratio are chosen. The general observation of the results reveal that the radius ratio and Brinkman number has significant impact on the heat transfer rate at the hot and cold walls. For all radius ratios and Brinkman numbers under consideration, the cold wall Nusselt number decreases

sharply with an increase in GR, while the hot wall Nusselt number increases with an increase in GR. For a chosen modified Grashof number and Brinkman number, the hot wall Nusselt number decreases with radius ratio, whereas the cold wall Nusselt number increases with radius ratio. This phenomenon can be anticipated due to the availability of larger annular space for smaller radius ratio. However, as the radius ratio increases, the width of annulus reduces and causes the reverse phenomenon. Further, in the presence of viscous dissipation, the hot wall Nusselt number reveals an interesting observation with modified Grashof number. It has been noted that the viscous dissipation effect causes significant decrease in the hot wall Nusselt number and is in accordance with the earlier literature findings.

The variation of thermal transport rate versus modified Grashof number for three different baffle positions is illustrated in Fig. 7 by setting other parameters as fixed. The modified Grashof number is varied from $GR = 50$ to 2000 whereas the baffle position is varied at three locations. The influence of baffle position on the rate of heat transport is important as compared to the modified Grashof number. The Nusselt number measured along the hot cylinder is higher for narrow annular passage or placing the baffle near hot wall and decreases as the baffle position moves toward cold or
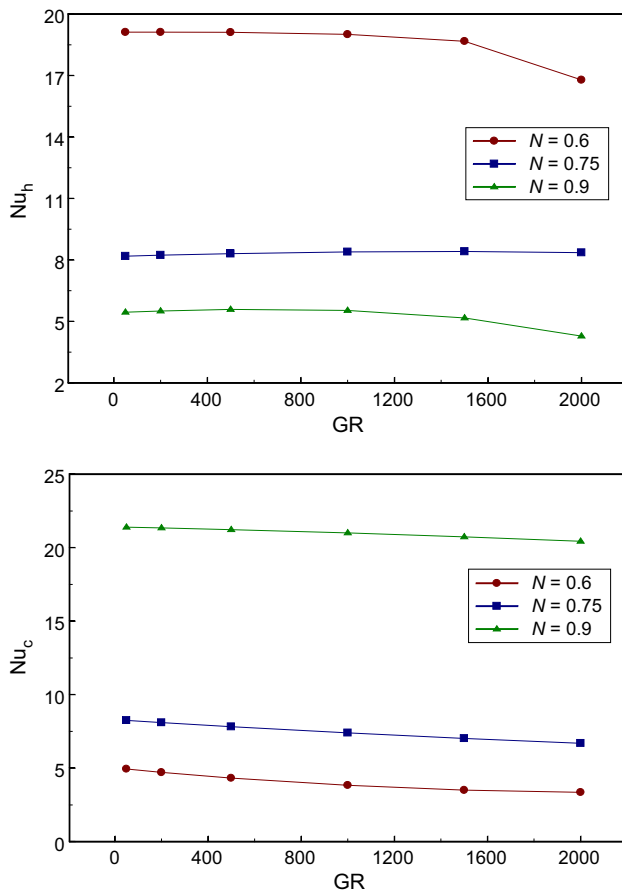
Fig. 7 Effect of *GR* and *N* on the hot (Nu_h) and cold (Nu_c) wall Nusselt numbers. For $\lambda = 0.5$ and $Br = 0.01$

outer wall. A similar trend is observed for Nusselt number at cold cylindrical wall, where Nu_c is higher for narrow passage near cold wall and the value of Nu_c decreases as baffle is moved toward hot wall. As regards to the *GR*, for any given baffle position, the Nusselt number measured along hot and cold walls meagerly varies with *GR*. A careful scrutiny of the heat transport variation reveals that for narrow and wider passages, the hot wall *Nu* abruptly reduces for $GR > 1500$. The plunge in the hot wall Nusselt number could be attributed to the effect of internal heating or viscous dissipation on fluid temperature. Interestingly, this trend is not reflected in the cold wall Nusselt number in all baffle positions.

Effect of viscous dissipation

In this section, viscous dissipation effect on velocity, temperature and Nusselt number profiles are discussed for various physical and geometrical parameters. The collective influence of Brinkman number and modified Grashof number on velocity and temperature field is shown in Fig. 8 for $\lambda = 0.5$ and $N = 0.75$. Here, three representative values of *Br* and *GR*

are considered. The velocity magnitude enhances with *GR* and *Br*, and this enhancement is significantly visible in both passages for $Br = 0.01$ but for $Br = 0.05$ and 0.075 velocity improvement is considerably higher in passage -2 compared to passage -1. For small values of Brinkman number ($Br = 0.01$), temperature profiles are linear in nature for all values of *GR*. However, as the value of *Br* increases, the temperature profile is significantly altered with *GR*. Among the parameters considered in this study, the maximum velocity and temperature is observed for $GR = 1000$ with $Br = 0.075$. In general, the influence of Brinkman number is dominant in the outer passage compared to passage -1, and the onset of flow reversal is observed in outer annular passage for higher Brinkman number.

Figure 9 portrays the velocity and temperature profiles for various values of *GR*, *Br* and *N*. To analyze the collective effects of *GR* and *Br*, the velocity and thermal distributions are displayed by considering two representative values of *GR* and three values of *Br*. The velocity profiles are altered as *Br* increases, and a considerable variation is observed in wider passage, but meager change is noted in slender annular passage. The impacts of *Br* and *GR* are diminutive when baffle is placed in the middle of the annuli. As regards to thermal profiles, fluid temperature significantly increases with an increase in *Br* for $GR = 500$ when the baffle is near the hot wall. As the baffle location moves toward cold wall, the influence of *GR* on thermal profiles is not visible; however, a strong influence of *Br* can be observed from Fig. 9.

Figure 10 displays the thermal transport rate variation with viscous dissipation and radius ratio for a fixed value of *GR* and *N*. The careful observation of the results show that the Nusselt number at hot cylinder decline to attain negative values at a critical *Br* and then increases to positive value. The negative values of hot wall Nusselt number signifies that the heat transfer is from fluid to cylindrical wall. An increase in the Brinkman number modifies the net heat balance, and hence, the internal heat generated by the viscous dissipation process may affect the uniform heating of inner cylindrical wall, resulting in negative Nusselt number. The cold wall Nusselt number is positive for all values of *Br*; however, (Nu_c) reveals the opposite behavior.

The collective effects of Brinkman number and baffle location on hot and cold wall Nusselt numbers are depicted in Fig. 11. The results revealed that the cold wall Nusselt number increases significantly with increase in *N* and *Br*. For all positions of the baffle, the hot wall Nusselt number sharply decreases to a negative value as *Br* increases from $Br = 0$ to 0.07 and then raises to a positive value. As explained earlier, this negative value of Nusselt number is due to the presence of viscous dissipation through the Brinkman number.
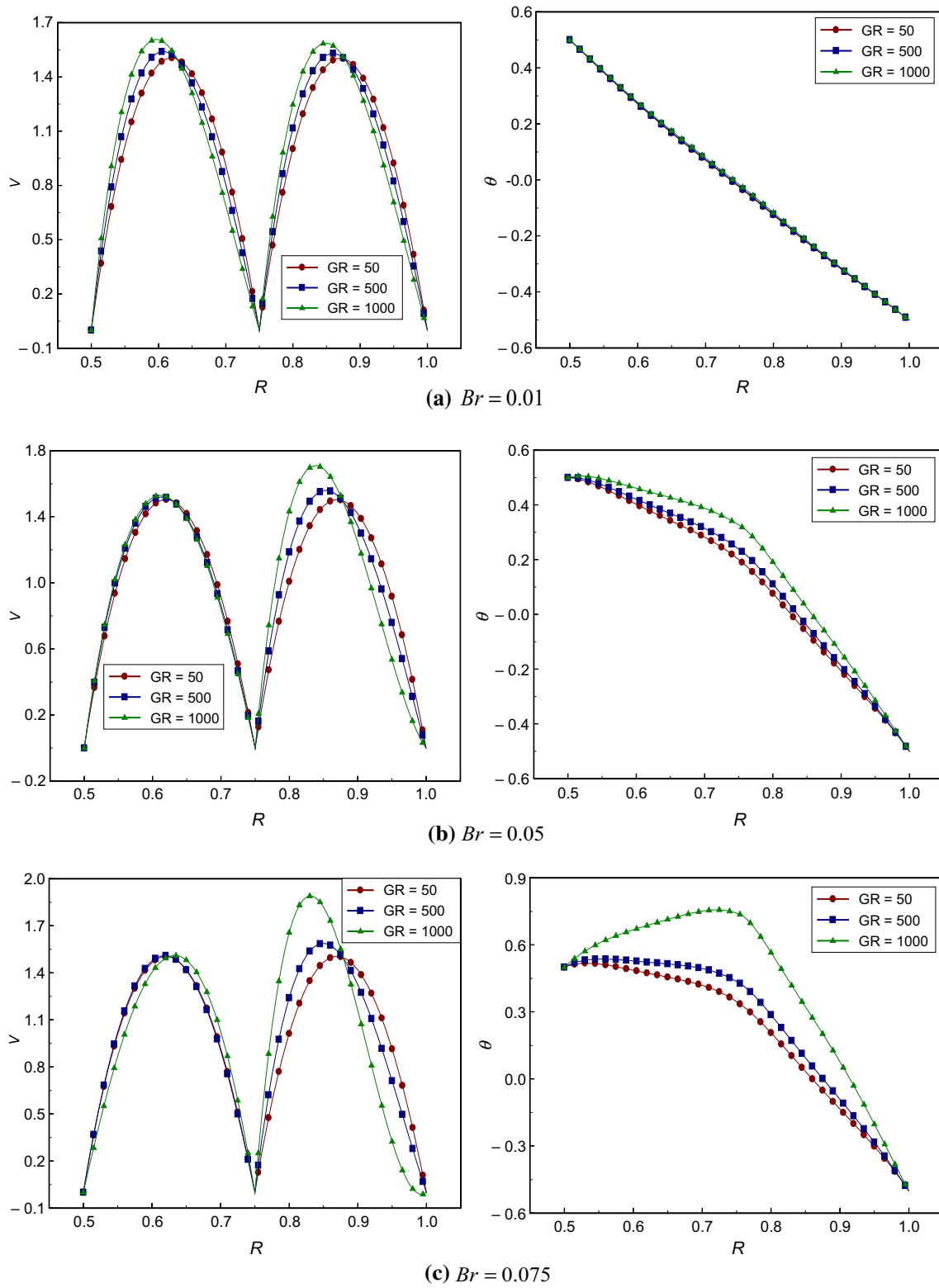
Fig. 8 Effects of *Br* and *GR* on velocity and temperature profiles for $\lambda = 0.5$ and $N = 0.75$

(a) $N = 0.6$

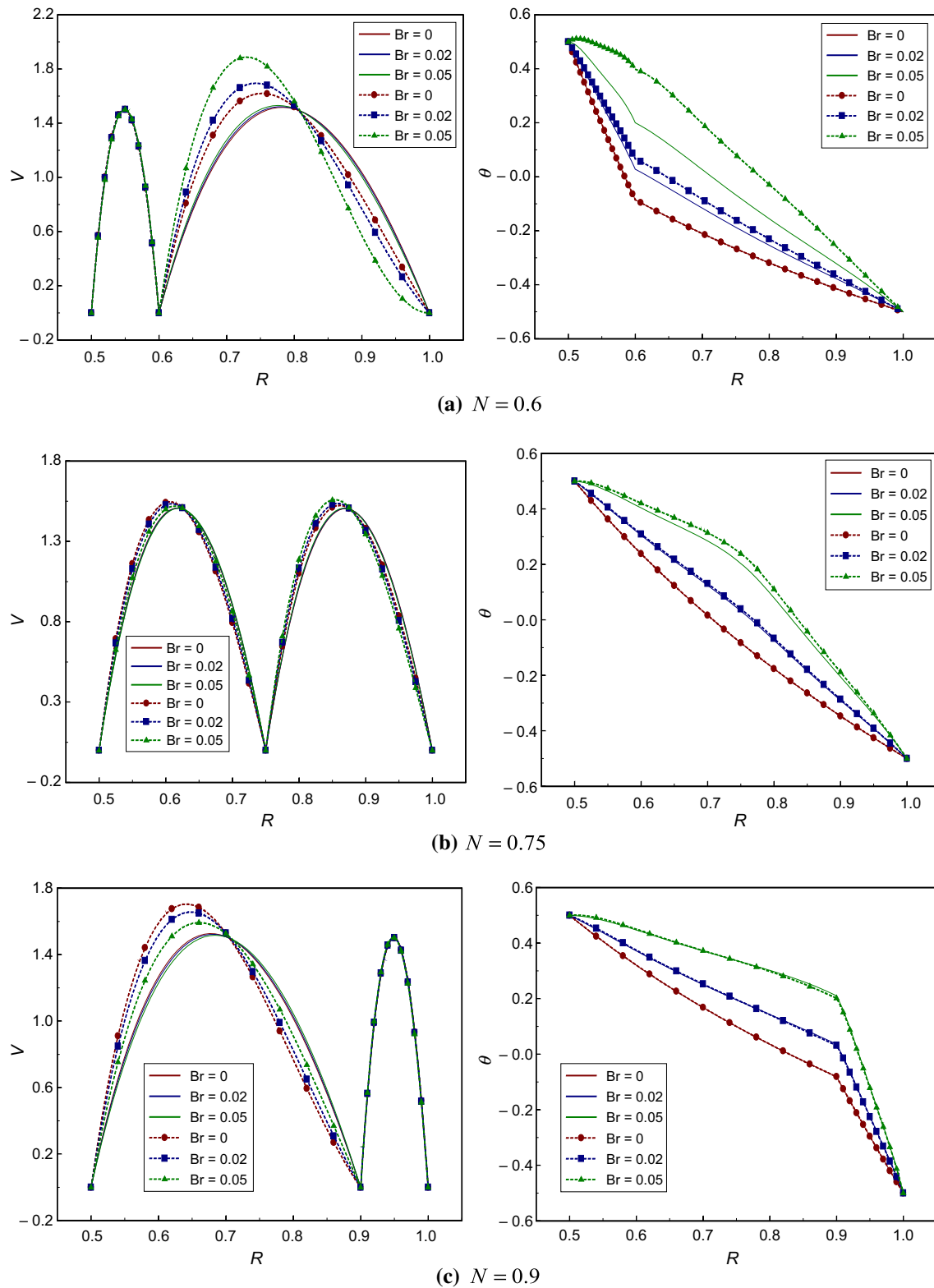**(b)** $N = 0.75$

(c) $N = 0.9$

Fig. 9 Velocity and temperature profiles for different values of baffle position (N), Brinkman number (BR) at $\lambda = 0.5$ and $GR = 100$ and 500. The continuous curves correspond to $GR = 100$ and discontinuous curves correspond to $GR = 500$
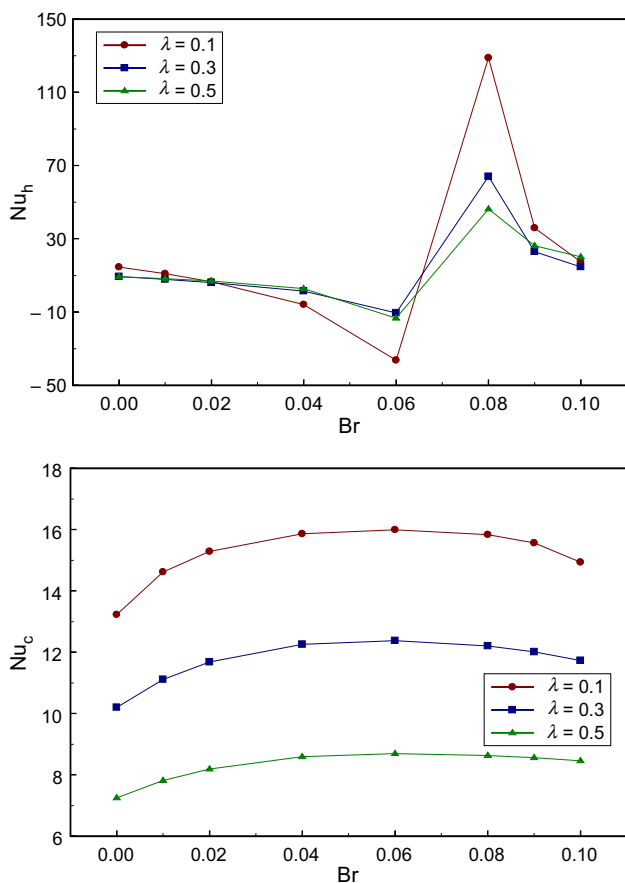
Fig. 10 Effect of Br and λ on the hot wall $\left(Nu_{\mathrm{h}}\right)$ and cold wall $\left(Nu_{\mathrm{c}}\right)$ Nusselt numbers for $GR = 500$ and $N = 0.75$

Fig. 11 Effect of Br and N on the hot wall $\left(Nu_{\mathrm{h}}\right)$ and cold wall $\left(Nu_{\mathrm{c}}\right)$ Nusselt numbers for $\lambda = 0.5$ and $GR = 100$

Effect of radius ratio

The effect of both geometric parameters, namely the radius ratio and baffle position on velocity and thermal distributions as well as Nusselt number, are illustrated in Figs. 12 and 13 by fixing all physical parameters.

The unequal passage widths are obtained by considering three different values for both baffle position and radii ratio. Figure 12 reveals that the velocity raises in passage -1 and drops in passage -2 when baffle moves toward cold wall for all the values of λ; however, decline in the magnitude of velocity is observed as λ increases. The effect of baffle position on thermal field is significant compared to radii ratio.

The effects of λ and N on heat transport rate are portrayed in Fig. 13. In general, cold wall Nusselt number increases with an increase in N and decrease in λ, whereas opposite situation is observed in case of hot wall Nusselt number except at $N = 0.6$. Particularly, cold wall Nusselt number increases suddenly for $N > 0.8$ for all the values of λ considered in the present study. The Nusselt number measured along hot and cold cylinders for different values of GR and Br, given in Table 2, predicts that the Nusselt number along
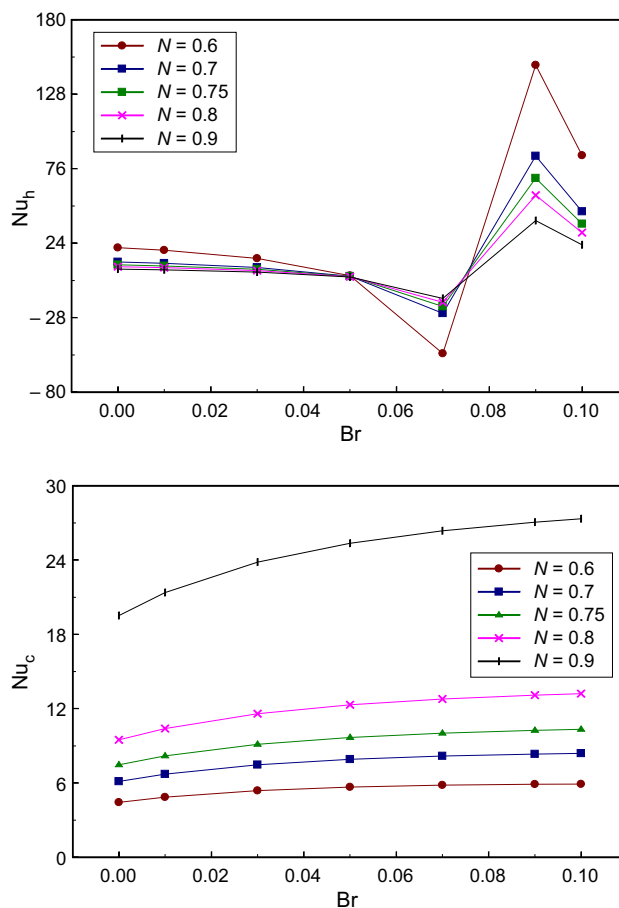
hot cylinder shows increasing trend with GR and decreases with Br; however, opposite trend is observed for cold wall Nusselt number.

Skin friction

The non-dimensional local surface shear stress coefficient along the innermost $(R = \lambda)$ and outermost $(R = 1)$ cylindrical surfaces is estimated through the skin friction coefficient for different combination of physical and geometrical parameters and are provided in Table 3. Generally, it is observed that the skin friction is more pronounced at the inner cylinder compared to outer cylinder for all parameter values and this prediction is consistent with the observations of Makinde [48]. Also, the skin friction increases with modified Grashof number, while decreases with Brinkman number, radius ratio and baffle position at the inner wall. Interestingly, the shear stress coefficient increases at the outer wall as the baffle move towards the outer cylinder.
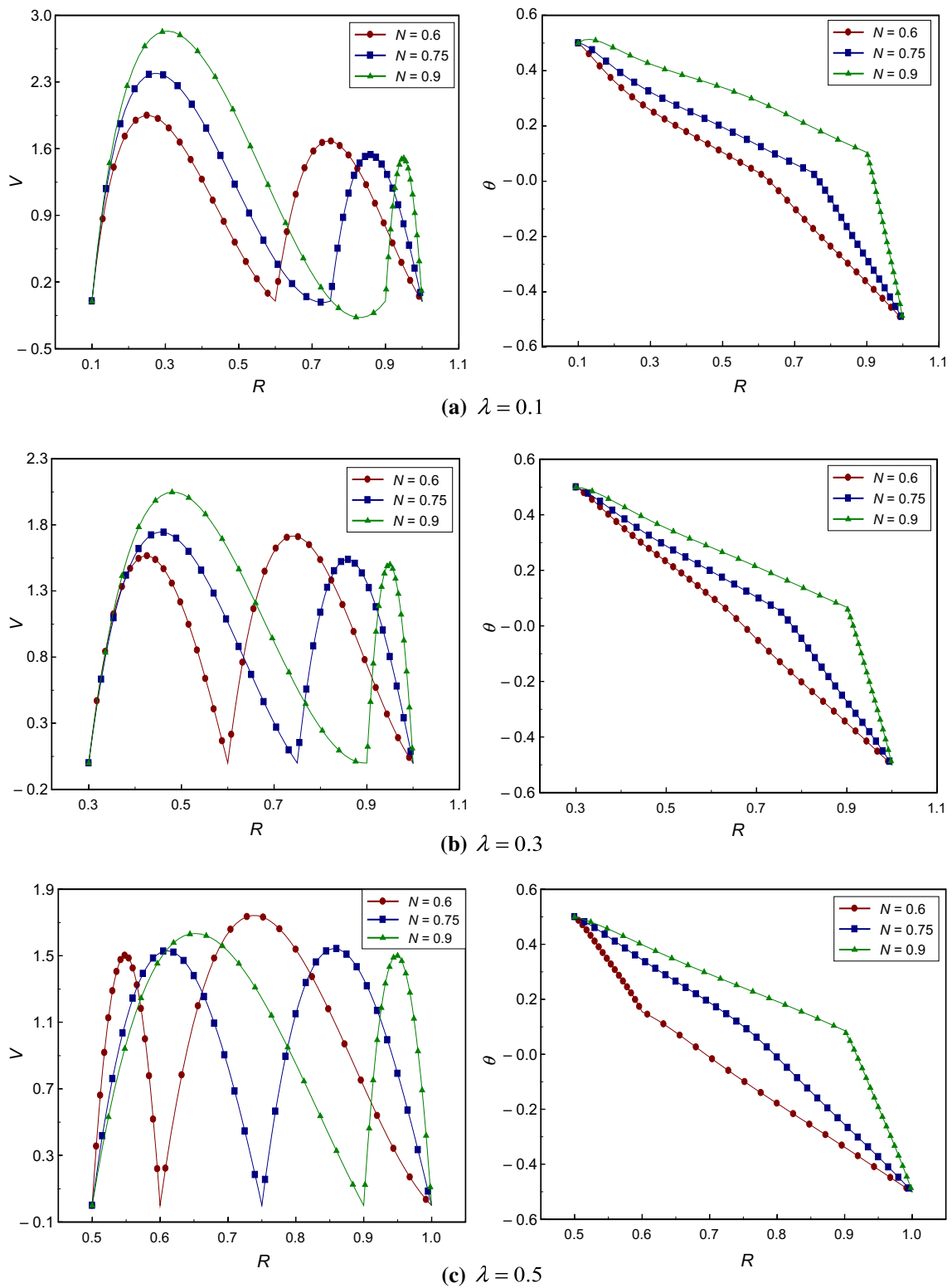
(a) $\lambda = 0.1$

(b) $\lambda = 0.3$

(c) $\lambda = 0.5$

Fig. 12 Effect of baffle position on velocity and temperature profiles for $GR = 500$ and $Br = 0.03$ different values of λ
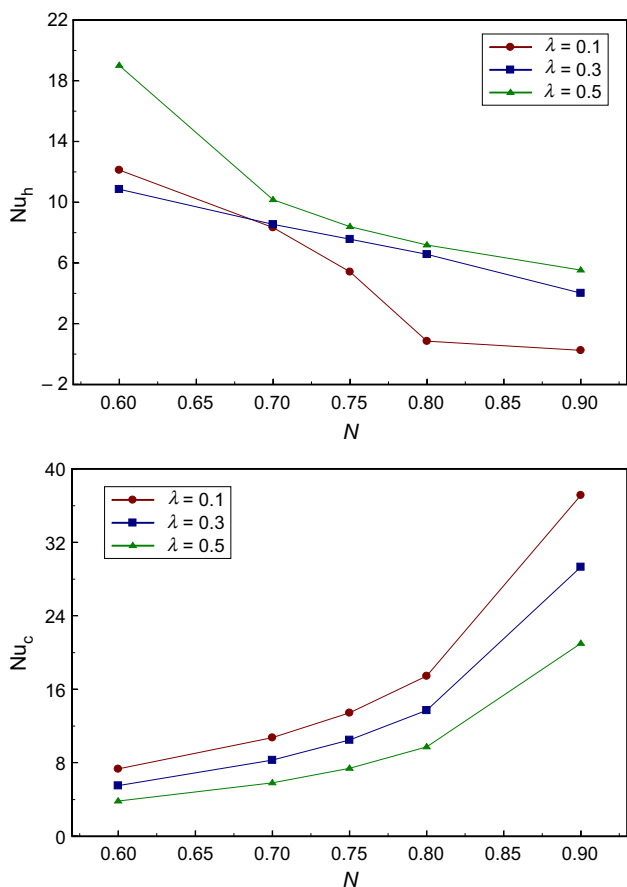
Fig. 13 Effect of λ and N on the hot wall (Nu_h) and cold wall (Nu_c) Nusselt numbers for $GR = 1000$ and $Br = 0.01$

Table 2 Variation of hot and cold wall Nusselt numbers for $\lambda = 0.5$ and $N = 0.75$ at different values of GR

	Nu_h			
	$GR = 100$	$GR = 500$	$GR = 1000$	$GR = 1500$
$Br = 0.0$	8.977220	9.311382	9.765781	10.266814
$Br = 0.01$	8.204175	8.307965	8.393412	8.417518
$Br = 0.02$	7.198752	7.039067	6.689912	6.141350
$Br = 0.03$	5.839376	5.400159	4.435879	2.820764
$Br = 0.04$	3.965370	2.876553	0.421526	− 7.516007
$Br = 0.042$	3.464051	2.192747	− 0.862413	− 15.478732
$Br = 0.050$	0.854505	− 1.667956	− 11.660115	21.700422
	Nu_c			
	$GR = 100$	$GR = 500$	$GR = 1000$	$GR = 1500$
$Br = 0.0$	7.474318	7.251984	6.991999	6.750009
$Br = 0.01$	8.198307	7.821097	7.398483	7.023577
$Br = 0.02$	8.726396	8.193984	7.608355	7.107239
$Br = 0.03$	9.125374	8.442296	7.697693	7.079095
$Br = 0.04$	9.443099	8.594294	7.683073	6.962141
$Br = 0.042$	9.496347	8.615026	7.671139	6.931461
$Br = 0.05$	9.685838	8.673277	7.598464	6.786307

Table 3 Variation of skin friction at inner and outer walls for different values of GR, Br, λ and N

GR	Br	λ	N	$(f \cdot Re)_{R=\lambda}$	$(f \cdot Re)_{R=1}$
50	0	0.5	0.75	53.20844737	45.16788002
100				54.56892824	44.37260402
500				65.45277515	38.01039598
1000				79.05758379	30.05763594
2000				106.26720108	14.15211586
500	0	0.5	0.75	65.45277515	38.01039598
	0.001			65.30737181	37.88519760
	0.05			57.53566383	31.14830106
	0.075			52.66873859	26.89995256
	0.1			46.85059999	21.79262980
1000	0.01	0.5	0.6	132.28563386	− 2.91760012
			0.7	82.39005757	15.45715565
			0.75	75.80424243	27.19957236
			0.8	73.31059420	42.84037496
			0.9	74.05535649	110.16318671
1000	0.01	0.1	0.75	134.24661812	28.21729219
		0.3		85.25376699	28.54487462
		0.5		75.80424243	27.19957236

Conclusions

Fully developed mixed convective flow and associated thermal transport in the vertical double annular passages is analyzed by considering viscous dissipation effects. The exact solutions are found for flow and thermal distributions as well as thermal transport across thermally active boundaries for situations of negligible viscous dissipation. It has been observed that the control parameters of the problem have intensive impacts on velocity and temperature fields, heat transport rate. In particular, the following conclusions are drawn based on the detailed analysis:

(a) For negligible viscous dissipation effects, modified Grashof number significantly alters the velocity field, but thermal field remains unchanged.

(b) For sufficiently large value of modified Grashof number, flow reversal occurs in the wider passage.

(c) The maximal velocity appears in wider annular passage and minimal velocity occurs in the slender passage for all radius ratios.

(d) Brinkman number strongly influences the temperature profiles; however, its effect on velocity profiles is moderate.

(e) The thermal transport rate on hot wall enhances with modified Grashof number but decrease with radius ratio in the absence of viscous dissipation.

(f) The rate of heat transfer on cold wall increase with increase in N but it decreases with increase in GR and λ in the absence or negligible viscous dissipation.

(g) Flow reversal is observed when one of the passages is narrow compared to equal passages and maximum velocity appears in wider passage.

(h) Nusselt number along hot cylinder reduces with Br for slender or wider passages.

(i) It is worth to mention that the present study is limited to the fully developed flow situations only. However, this analysis can be extended to developing flow regimes for different type of fluids.

References

1. McBain GD. Fully developed laminar buoyant flow in vertical cavities and ducts of bounded section. J Fluid Mech. 1999;401:365–77.

2. El-Din MMS. Fully developed forced convection in a vertical channel with combined buoyancy forces. Int. Commun. Heat Mass Transf. 1992;19(2):239–48.

3. Guo ZY, Li DY, Wang BX. A novel concept for convective heat transfer enhancement. Int J Heat Mass Transf. 1998;41(14):2221–5.

4. Tso CP, Mahulikar SP. The use of the Brinkman number for single phase forced convective heat transfer in microchannels. Int J Heat Mass Transf. 1998;41(12):1759–69.

5. Barletta A. Laminar mixed convection with viscous dissipation in a vertical channel. Int J Heat Mass Transf. 1998;41(22):3501–13.

6. Barletta A, Zanchini E. On the choice of the reference temperature for fully-developed mixed convection in a vertical channel. Int J Heat Mass Transf. 1999;42(16):3169–81.

7. Barletta A, Zanchini E. Mixed convection with viscous dissipation in an inclined channel with prescribed wall temperatures. Int J Heat Mass Transf. 2001;44(22):4267–75.

8. Avci M, Aydin O. Mixed convection in a vertical parallel plate microchannel with asymmetric wall heat fluxes. J Heat Transf. 2007;129(8):1091–5.

9. Umavathi JC, Chamkha AJ. Fully developed mixed convection in a vertical channel in the presence of heat source or heat sink. Int J Energy Technol. 2011;3(24):1–9.

10. Idowu AS, Joseph KM, Onwubuoya C, Joseph WD. Viscous dissipation and buoyancy effects on laminar convection in a vertical channel with transpiration. Int J Appl Math Res. 2013;2(4):455–63.

11. Roy K, Murthy PVSN. Effect of viscous dissipation on the convective instability induced by inclined temperature gradients in a non-Darcy porous medium with horizontal throughflow. Phys Fluids. 2017;29(4):044104–12.

12. Malvandi A, Ganji DD, Kaffash MH. Magnetic field effects on nanoparticle migration and heat transfer of alumina/water nanofluid in a parallel-plate channel with asymmetric heating. Eur Phys J Plus. 2015;130(63):1–21.

13. Khan I, Khan WA. Effect of viscous dissipation on MHD water-Cu and EG-Cu nanofluids flowing through a porous medium: a comparative study of Stokes second problem. J Therm Anal Calorim. 2019;135(1):645–56.

14. Smith AN, Nochetto H. Laminar thermally developing flow in rectangular channels and parallel plates: uniform heat flux. Heat Mass Transf. 2014;50(11):1627–37.

15. Morton BR. Laminar convection in uniformly heated vertical pipes. J Fluid Mech. 1960;8(2):227–40.

16. Barletta A. Fully developed laminar forced convection in circular ducts for power-law fluids with viscous dissipation. Int J Heat Mass Transf. 1996;40(1):15–26.

17. Barletta A. Combined forced and free convection with viscous dissipation in a vertical circular duct. Int J Heat Mass Transf. 1999;42(12):2243–53.

18. Lee K-T. Fully developed laminar natural convection heat and mass transfer in partially heated vertical pipe. Int Commun Heat Mass Transf. 2000;27(7):995–1001.

19. Jha BK, Samaila AK, Ajibade AO. Transient free-convective flow of reactive viscous fluid in vertical tube. Math Comput Model. 2011;54(11–12):2880–8.

20. Rokerya MS, Iqbal M. Effects of viscous dissipation on combined free and forced convection through vertical concentric annuli. Int J Heat Mass Transf. 1971;14(3):491–5.

21. Prakash C, Renzoni P. Effect of buoyancy on laminar fully developed flow in a vertical annular passage with radial internal fins. Int J Heat Mass Transf. 1985;28(5):995–1003.

22. Herwig H, Klemp K. Variable property effects of fully developed laminar flow in concentric annuli. ASME J Heat Transf. 1988;110(2):314–20.

23. El-Shaarawi MAI, Al-Nimr MA. Fully developed laminar natural convection in open-ended vertical concentric annuli. Int J Heat Mass Transf. 1990;33(9):1873–84.

24. Al-Nimr MA. Analytical solution for transient laminar fully developed free convection in vertical concentric annuli. Int J Heat Mass Transf. 1993;36(9):2385–95.

25. Coelho PM, Pinho FT. Fully-developed heat transfer in annuli with viscous dissipation. Int J Heat Mass Transf. 2006;49(19–20):3349–59.

26. Jha BK, Samaila AK, Ajibade AO. Unsteady/steady natural convection flow of reactive viscous fluid in a vertical annulus. Int J Appl Mech Eng. 2013;18(1):73–83.

27. Jha BK, Aina B, Rilwanu Z. Steady fully developed natural convection flow in a vertical annular microchannel having temperature dependent viscosity: an exact solution. Alex Eng J. 2016;55(2):951–8.

28. Sankar M, Girish N, Siri Z. Fully developed magnetoconvective heat transfer in vertical double-passage porous annuli. In: Narayanan N, Mohanadhas B, Mangottiri V, editors. Flow and transport in subsurface environment. Singapore: Springer; 2018. p. 217–49.

29. Girish N, Makinde OD, Sankar M. Numerical investigation of developing natural convection in vertical double-passage porous annuli. Defect Diffus Forum. 2018;387:442–60.

30. Girish N, Sankar M, Do Y. Numerical investigation of developing laminar convection in vertical double-passage annuli. In: Rushikumar B, Sivaraj R, Prasad B, Nalliah M, Reddy A, editors. Applied mathematics and scientific computing, trends in mathematics. Cham: Birkhäuser; 2019. p. 407–15.

31. Sheikholeslamia M, Gorji-Bandpy M, Ganji DD. Fluid flow and heat transfer in an air-to-water double-pipe heat exchanger. Eur Phys J Plus. 2015;130(225):1–12.

32. Raei B, Shahraki F, Jamialahmadi M, Peyghambarzadeh SM. Experimental study on the heat transfer and flow properties of γ-Al_2O_3/water nanofluid in a double-tube heat exchanger. J Therm Anal Calorim. 2017;127(3):2561–75.

33. Raj AK, Kunal G, Srinivas M, Jayaraj S. Performance analysis of a double-pass solar air heater system with asymmetric channel flow passages. J Therm Anal Calorim. 2019;136(1):21–38.

34. El-Din MMS. Fully developed laminar convection in a vertical double-passage channel. Appl Energy. 1994;47(1):69–75.

35. El-Din MMS. Effect of viscous dissipation on fully developed laminar mixed convection in a vertical double-passage channel. Int J Therm Sci. 2002;41(3):253–9.

36. El-Din MMS. Laminar fully developed mixed convection with viscous dissipation in a uniformly heated vertical double-passage channel. Therm Sci. 2007;11(1):27–41.

37. Umavathi JC. Mixed convection of micropolar fluid in a vertical double-passage channel. Int J Eng Sci Technol. 2011;3(8):197–209.

38. Ahmed F, Iqbal M, Ioan P. Numerical simulation of forced convective power law nanofluid through circular annulus sector. J Therm Anal Calorim. 2019;135(2):861–71.

39. Malvandi A, Moshizi SA, Ganji DD. Effect of magnetic fields on heat convection inside a concentric annulus filled with Al_2O_3–water nanofluid. Adv Powder Technol. 2014;25(6):1817–24.

40. Mebarek-Oudina F. Numerical modeling of the hydrodynamic stability in vertical annulus with heat source of different lengths. Eng Sci Technol Int J. 2017;20:1324–33.

41. Gourari S, Mebarek-Oudina F, Hussein AK, Kolsi L, Hassen W, Younis O. Numerical study of natural convection between two coaxial inclined cylinders. Int J Heat Technol. 2019;37(3):779–86.

42. Shakiba A, Rahimi AB. Nanofluid flow and MHD mixed convection inside a vertical annulus with moving walls and transpiration considering the effect of Brownian motion and shape factor. J Therm Anal Calorim. 2019;138(1):501–15.

43. Hekmat MH, Rabiee MB, Ziarati KK. Numerical investigation of the mixed convection of a magnetic nanofluid in an annulus between two vertical concentric cylinders under the influence of a non-uniform external magnetic field. J Therm Anal Calorim. 2019;138(2):1745–59.

44. Mebarek-Oudina F, Bessaïh R. Numerical simulation of natural convection heat transfer of copper-water nanofluid in a vertical cylindrical annulus with heat sources. Thermophys Aeromech. 2019;26(3):325–34.

45. Mebarek-Oudina F. Convective heat transfer of Titania nanofluids of different base fluids in cylindrical annulus with discrete heat source. Heat Transf Asian Res. 2019;48(1):135–47.

46. Singh G, Makinde OD. Axisymmetric slip flow on a vertical cylinder with heat transfer. Sains Malays. 2014;43(3):483–9.

47. Eegunjobi AS, Makinde OD. Entropy generation analysis in transient variable viscosity Couette flow between two concentric pipes. J Therm Sci Technol. 2014;9(2):1400217:1–11.

48. Makinde OD. Thermal analysis of a reactive generalized Couette flow of power law fluids between concentric cylindrical pipes. Eur Phys J Plus. 2014;129(270):1–9.

49. Khamis S, Makinde OD, Nkansah-Gyekye Y. Buoyancy - driven heat transfer of water based nanofluid in a permeable cylindrical pipe with Navier slip through a saturated porous medium. J Porous Media. 2015;18(12):1169–80.

50. Raza J, Mebarek-Oudina F, Chamkha A. Magnetohydrodynamic flow of molybdenum disulfide nanofluid in a channel with shape effects. Multidiscip Model Mater Struct. 2019;15(4):737–57.